



Published in final edited form as:

J Neurosci. 2010 October 20; 30(42): 13966–13976. doi:10.1523/JNEUROSCI.3637-10.2010.

Silencing of CDK5 Reduces Neurofibrillary Tangles in Transgenic Alzheimer's Mice

Diego Piedrahita¹, Israel Hernández^{1,6}, Alejandro López-Tobón¹, Dmitry Fedorov², Boguslaw Obara³, B.S. Manjunath², Ryan L Boudreau⁴, Beverly Davidson⁴, Frank LaFerla⁵, Juan Carlos Gallego-Gómez¹, Kenneth S. Kosik^{6,*}, and Gloria Patricia Cardona-Gómez^{1,*}

¹Cellular and Molecular Neurobiology Area, Viral Vector Core and Gene Therapy. Group of Neuroscience of Antioquia, Faculty of Medicine, SIU, University of Antioquia, Medellín, Colombia

²Center for Biomed Informatics, University of California, Santa Barbara, CA, USA

³Oxford e-Research Centre and Oxford Centre for Integrative Systems Biology, University of Oxford, Oxford, UK

⁴Viral Vector Core and Davidson Laboratory, University of Iowa, USA

⁵Institute for Brain Aging and Dementia, University of California in Irvine, USA

⁶Neuroscience Research Institute and Department of Molecular, Cellular and Developmental Biology, University of California Santa Barbara, USA

Abstract

Alzheimer's disease is a major cause of dementia for which treatments remain unsatisfactory. Cyclin-dependent kinase 5 (CDK5) is a relevant kinase that has been hypothesized to contribute to the tau pathology. Several classes of chemical inhibitors for CDK5 have been developed, but they generally lack the specificity to distinguish among various ATP-dependent kinases. Therefore, the efficacy of these compounds when tested in animal models cannot definitively be attributed to an effect on CDK5. However, RNA interference (RNAi) targeting of CDK5 is specific and can be used to validate CDK5 as a possible treatment target. We delivered a CDK5 RNAi by lentiviral (LV) or Adeno-Associated Viral Vectors (AAV) and analyzed the results *in vitro* and *in vivo*. Silencing of CDK5 reduces the phosphorylation of tau in primary neuronal cultures and in the brain of wild type C57BL/6 mice. Furthermore, the knock-down of CDK5 strongly decreased the number of neurofibrillary tangles in the hippocampi of triple transgenic mice (3xTg-AD mice). Our data suggest that this down-regulation may be due to the reduction of the CDK5 availability in the tissue, without affecting the CDK5 kinase activity. In summary, our findings validate CDK5 as a reasonable therapeutic target for ameliorating tau pathology.

Keywords

Alzheimer's disease; CDK5; PHF-1 Tau; NFTs; 3xTg-AD; Gene Therapy

*Corresponding authors: Gloria Patricia Cardona - Gómez, Universidad de Antioquia, Sede de Investigación Universitaria (SIU), Calle 62 # 52 – 59; Torre 1, Piso 4, Laboratorio 412; Medellín, Colombia. Phone: 57-4-2196458; Fax: 57-4-2196444; patricia.cardona@neurociencias.udea.edu.co. Kenneth S Kosik, Neuroscience Research Institute, University of California Santa Barbara. Biology II, Room 6139A. Santa Barbara, CA 93106. Phone: (805) 893-5222, Fax: (805) 893-2005, kosik@lifesci.ucsb.edu.

Introduction

Alzheimer's disease (AD) is a progressive neurodegenerative disorder, considered a major cause of dementia and a public health problem around the world. The main hallmarks of AD are β -amyloid extracellular plaques and intracellular tau pathology that appear progressively. Tau pathology is characterized by excessive tau phosphorylation, reduced binding affinity of tau to microtubules and the formation of aberrant tau aggregates known as neurofibrillary tangles (NFT). Because the presence and extent of NFTs has been correlated with the level of dementia (Arriagada et al., 1992), drugs which control the phosphorylation state of tau deserve attention (Iqbal et al., 2005). Several strategies have been tried to inhibit tau phosphorylation but with limited success (Churcher, 2006; Skovronsky et al., 2006; Mazanetz and Fischer, 2007).

Nineteen phosphorylation sites have been identified in tau associated with paired helical filaments (PHF) (Morishima-Kawashima et al., 1995; Augustinack et al., 2002; Yu et al., 2009). *In vitro* experiments have demonstrated that tau is a substrate for several kinases (Kobayashi et al., 1993; Paudel et al., 1993; Patrick et al., 1999). Cyclin-dependent kinase 5 (CDK5) has been considered a major tau kinase that contributes to tau pathology (Baumann et al., 1993; Paudel et al., 1993).

CDK5 is a serine threonine kinase with pleiotropic effects in the mammalian central nervous system (CNS) (Dhavan and Tsai, 2001). Interaction of CDK5 with either p35 or p39, two proteins abundantly expressed in post-mitotic neurons, is necessary for its activation (Lew et al., 1994; Tsai et al., 1994; Tang et al., 1995). Cleavage of p35 to a truncated form, p25, by calpain delocalizes and deregulates CDK5 (Kusakawa et al., 2000). The aberrant activity of CDK5 by p25 has been associated with NFTs (Cruz et al., 2003; Noble et al., 2003).

Several classes of potent chemical inhibitors for CDK5 have been reviewed (Fischer, 2001). Most of them are competitive inhibitors at the ATP binding site, resulting in a lack of specificity among kinases (Garrett and Fattaey, 1999; Gray et al., 1999; Meijer et al., 1999; Leost et al., 2000; Sielecki et al., 2000; Fischer, 2001; Knockaert et al., 2002; Mettey et al., 2003). Discovery of more specific CDK5 inhibitors could be a useful therapeutic (Shiradkar et al., 2007; Gong and Iqbal, 2008). However, before undertaking this onerous task one would like better evidence that CDK5 is a reasonable treatment target. In the present study, we used RNAi to target CDK5 with very high specificity and evaluated its effect on the phosphorylation of tau and on the tau pathology, using a triple transgenic mice model of Alzheimer's disease.

Materials and Methods

RNAi Design

The RNAi (Short hairpin RNAmiR, shRNAmiR) sequences for silencing of CDK5 (shRNAmiR-CDK5) and a scrambled RNA sequence as control (shRNAmir-SCR) were based on previously published sequences (Chang et al., 2006). These sequences were cloned into human miR-30-based stem-loops by polymerase extension of overlapping DNA oligonucleotides. For cloning of lentiviral (LV) RNAi constructs, the following primers were used for polymerase extension: shCDK5miR forward primer 5' CAGAAGGCTCGAGAAGGTATATGCTGTTGACAGTGAGCGACATGACCAAGCTGCCAGACTATAGTGAAGCCACAGATGTA 3' and shCDK5miR reverse primer 5' CTAAAGTAGCCCCCTTGAATTCCGAGGCAGTAGGCACCATGACCAAGCTGCCAGACTATACATCTGTGGCTTCAC 3' or shSCRmiR forward primer 5' CAGAAGGCTCGAGAAGGTATATGCTGTTGACTAGCACACATCAGGAAGCGCTCGACAGTGATAGTGAAGCCACAGATGTA 3' and shSCRmiR reverse primer 5'

CTAAAGTAGCCCCTTGAATTCCGAGGCAGTAGGCACCTAGCACACATCAGGAAGCGCTCGACAGTGATACATCTGTGGCTTCAC 3'. The extension products were digested with XhoI and EcoRI for directional cloning into the vector pCMV-GIN-ZEO.GFP (Open Biosystems). For cloning of RNAi vectors for AAV production, the following primers were used for polymerase extension: shCDK5miR forward primer 5' AAAACTCGAGTGAGCGCTGACCAAGCTGCCAGACTATACTGTAAAGCCACAGATGGG 3' and shCDK5miR reverse primer 5' AAAAAGTACTAGTGGCGTTGACCAAGCTGCCAGACTATACCCATCTGTGGCTTTACAG 3' or shSCRmiR forward primer 5' AAAACTCGAGTGAGCGCACCATCGAACCGTCAGAGTTACTGTAAAGCCACAGATGGG 3' and shSCRmiR reverse primer 5' AAAAAGTACTAGTGGCGTACCATCGAACCGTCAGAGTTACCCATCTGTGGCTTTACAG 3'. These extension products were digested with XhoI and SpeI for directional cloning into a U6 expression plasmid cut with XhoI and XbaI (Boudreau et al., 2008).

Viral Particle Production

To produce lentiviral particles, the plasmid pCMV-GIN-ZEO.GFP (Open Biosystems) (Silva et al., 2005; Stegmeier et al., 2005), which coexpressed Green Fluorescent Protein (GFP) and the designed miRNA was cloned. The lentivirus vector was produced by cotransfection of 10-cm plates of highly confluent HEK-293T cells (Human Embryonic Kidney 293 cells) with 30 µg of vector core plasmid pCMV-GIN-ZEO.GFP, 27 µg of Packaging plasmid psPAX2 (Addgene, plasmid #12260), and 3 µg of VSV-G Envelope Plasmid pMD2G (Addgene, plasmid # 12259) using Calcium Phosphate (Zufferey and Trono 2000). Supernatant of conditioned medium was collected at 48 h following transfection. The supernatant was clarified by filtering through a 0.45µm filter. The viral particles were concentrated by ultracentrifugation at 30,000 rpm for 2 h at 4 °C with a Beckman 50TI rotor on a 20% sucrose cushion. The viral pellet was re-suspended in 200 µL of 1× PBS and titered by HIV p24 ELISA, Lentivirus Quantitation Kit (Cell Biolabs, Inc) and transducing units (TU/mL) in HEK-293T (Naldini et al., 1996).

The protocol to produce AAV particles was for large-scale production of heterologous proteins by Sf9 insect cells culture for co-infecting recombinant baculovirus derived from the *Autographa californica* nuclear polyhedrosis virus (Urabe et al., 2002). The shRNAmir-CDK5 and shRNAmir-SCR expression cassettes – driven by the mouse U6 promoter – were cloned into pAAV.CMV.hrGFP, which contains AAV serotype 2/5 inverted terminal repeats, and a CMV-humanized *Renilla* GFP (hrGFP)-simian virus 40 poly (A) reporter cassette (Boudreau et al., 2009; Urabe et al., 2002). AAV titers were determined by using quantitative PCR and/or DNA slot blot analysis. The AAV were dialyzed before use.

Transfections and Transductions

Hippocampal and cortical primary cultures from C57BL/6 mice or Wistar rat embryos (E17–18) were dissected, trypsinized, dissociated (Banker and Kimberly 2002) and cultured at a density of 5×10^5 cells on poly-L-Lysine (Sigma-Aldrich) pre-coated 24-well or 6-well plates in Neurobasal medium (GIBCO) containing B-27 supplement, (Sigma-Aldrich), and Penicillin-Streptomycin antibiotic mixture (GIBCO), at 37 °C and 5% CO₂ in a humidified atmosphere.

Transient transfection with lentiviral vector plasmid was done in HEK293T cells at Day *in vitro* 3 (DIV3) and neuronal primary cultures at DIV5 using Lipofectamine 2000 according to the manufacturer's instructions (Invitrogen). At DIV5 neuronal primary cultures plated in 6/well plates were transduced for 3 days with 2 µL of LV with a titre of 10^9 Lentiviral Particles per mL or for 15 days with 2 µL of AAV with a titre of 10^{12} genomes per mL.

Western Blotting

Neuronal primary cultures, HEK-293T cell or hippocampal samples were lysed on 150 mM NaCl, 20 mM Tris, pH 7.4, 10% glycerol, 1 mM EDTA, 1% NP-40, 100 μ M phenylmethylsulfonyl fluoride, 1 μ g/mL aprotinin and leupeptin (Sigma) and 100 μ M orthovanadate (Cardona-Gomez et al., 2004). Proteins were loaded on 10% SDS-PAGE gel and transferred to nitrocellulose membranes (Amersham) at 250 mA for 2 h using an electrophoretic transfer system. The membranes were incubated overnight at 4 °C with rabbit anti-CDK5 (C-8) (1:1000, Santa Cruz Biotechnology), PHF-1 monoclonal antibody which recognizes Tau phospho-Ser-396/404 donated by P. Davies (Feinstein Institute for Medical Research, Manhasset, NY), rabbit anti-p35/p25 (C-19) (1:1000, Santa Cruz Biotechnology), total tau (tau-5) (1:1000, Invitrogen) and mouse anti- β Actin (1:2000, Sigma-Aldrich). IRDye 800CW Goat Anti-Mouse or rabbit (LI-COR, Inc, diluted 1:5000) and anti-mouse IgG or anti-rabbit IgG, peroxidase conjugated (Jackson Laboratories, diluted 1:10000) were used as secondary probes. The blots were developed using The Odyssey® Infrared Imaging System or chemiluminescence method (ECL Western blotting system, Amersham) followed by an exposure to a radiographic film (ECL Hyperfilm, Amersham). The films were analyzed using Quantity One version 4.3.0 (Biorad).

Immunofluorescence

Cell cultures were fixed 20 minutes in 4% paraformaldehyde in cytoskeleton buffer (CB) (Gallego-Gomez et al., 2003). Autofluorescence was reduced with 50 mM NH_4Cl . Cells were permeabilized and blocked with 0.1% PBS Triton X-100 and 1% bovine serum for 1 h. Cultures were incubated overnight at 4 °C with primary antibodies, rabbit anti-CDK5 (C-8) (1:1000, Santa Cruz Biotechnology, inc), and mouse anti-Human-PHF-Tau (AT-8, clone which recognizes Tau phospho-Ser-202/Thr205, 1:500, Pierce Biotechnology). We used Alexa 488, and Alexa 594 secondary fluorescent antibodies (Molecular Probes) during 1 h and the nuclei were stained with Hoechst (1:5000, Invitrogen) for the last 15 min. The cells were observed by fluorescence microscopy (Olympus IX81). The images were analyzed individually to evaluate GFP, CDK5, and AT-8 immunoreactive expression and the fluorescent intensity per area selected (soma or dendritic processes) was determined in 30 neurons per assay by software Image Scope Pro, MediaCybernetics®.

Mouse brains were cut in 50 μ m coronal sections with a vibratome (Leica 1000) and treated with 50 mM NH_4Cl for 10 min at room temperature. Slices were pre-incubated 1 h in 1% BSA with 0.3% Triton X-100 in 0.1 M PB. Primary antibodies were incubated overnight at 4 °C. We used rabbit anti-CDK5 (C-8) (1:500, Santa Cruz Biotechnology), and PHF-1 antibody. Alexa 488, and Alexa 594 were used as secondary fluorescent probes. The slices were observed by fluorescence microscopy Olympus IX-81 or Olympus FV-1000 CLS, and analyzed as individual images for GFP, CDK5 and PHF-1 expression. Deconvolution and fluorescence intensity were done using Image Scope pro software (Media Cybernetics) and Cell Software (Olympus).

Animal Procedures

Neuronal primary cultures were prepared from pregnant C57BL6 mice or Wistar rats at embryonic days 17–18 (E17–E18) housed in the vivarium at SIU-University of Antioquia, Medellín, Colombia. Animals were handled following the Colombian regulations (Law 84 of 1989 and resolution 8430 of 1993) and the NIH animal welfare care guidelines (Public Law 99–158, November 20, 1985, “Animals in Research”). A total of twenty 6 month old C57BL/6 wild type mice and forty two 18–23 month old triple transgenic Alzheimer mice (3xTg-AD) were used (Oddo et al., 2003).

Animals were injected with 2 μL of AAV2-shRNAmirSCR (SCRmiR), or AAV2-shRNAmirCDK5 into the right hippocampus (Bregma Coordinates were -1.7 antero-posterior, -0.7 lateral and -1.75 depth). For CDK5 kinase activity measurements the mice were bilaterally injected into the hippocampus with the viral vectors. Injections were performed with a 10 μL Hamilton syringe at a rate of 0.2 $\mu\text{L}/\text{min}$ and 5 min elapsed after infusion before withdrawal of the syringe. Animals were perfused transcardially with 4% paraformaldehyde in PBS and processed for the immunodetection. The brains were cryopreserved with 30% sucrose and stored at $-20\text{ }^{\circ}\text{C}$. For biochemical measures the hippocampi were dissected and immediately frozen on dry ice and stored at $-80\text{ }^{\circ}\text{C}$ before use.

In vitro CDK5 Kinase Assay

Three weeks after stereotactic injection of AAV2-CDK5miR or AAV2-SCRmiR into the hippocampus of 3xTg-AD and C57BL/6 wild type mice, the animals were sacrificed and the hippocampi were dissected, placed on a 1.5 mL microfuge tube containing lysis buffer, and rapidly frozen in liquid Nitrogen immersion. Brain tissue was kept at $-70\text{ }^{\circ}\text{C}$ to preserve enzymatic activity until the assay was performed. Brain tissue was thawed on ice and homogenized, incubated for 15 min on ice, and centrifuged at 13,000 rpm/ $4\text{ }^{\circ}\text{C}$. Supernatant was recovered in clean microfuge tubes and protein concentration was measured with the bicinchonic acid method (Thermo Scientific). CDK5 was immunoprecipitated from 250 μg of total protein using 1 μg of IgG rabbit polyclonal anti-CDK5 (C-8) antibody (Santa Cruz). Antibody and protein extract was incubated overnight at $4\text{ }^{\circ}\text{C}$ in a rotator; protein G sepharose (Sigma) was added and incubated for an additional 1h at $23\text{ }^{\circ}\text{C}$, protein G sepharose beads were washed 5 times with IP buffer (Sigma), keeping the sample at $4\text{ }^{\circ}\text{C}$. After the fifth wash, the protein G sepharose beads were re-suspended in 200 μL of kinase assay buffer (20 mM Tris/HCl pH 7.5, 100 μM sodium orthovanadate, 10 mM MgCl_2 , 50 mM NaCl, 1 mM DTT, and 1 mM NaF), and ATP was added to the re-suspended beads at a 10-fold excess (0.5 mM). Histone from Calf Thymus Type III-S (Sigma) was added as a substrate for CDK5 at a final concentration of 6 μM , and then the reaction was gently vortexed, and aliquoted in up to 8 fractions 25 μL each, and incubated at $37\text{ }^{\circ}\text{C}$, for times ranging from 15 to 60 min. To stop the reaction, 5 μL SDS-PAGE loading buffer (250 mM TrisHCl, 10% SDS, 30% Glycerol, 0.5 M DTT, 0.02% bromophenol blue) was added, immediately followed by 5 min incubation at $95\text{ }^{\circ}\text{C}$. The samples were separated electrophoretically at 120 V/2 h and transferred to a nitrocellulose membrane at 200 mA/1.5 h. Ponceau Red in 5% acetic acid was used to stain the transferred proteins. Histone was clearly visible, and its migration on the gel was identified around 21 KDa. Western blotting detection for CDK5 (C-8 antibody) and rabbit polyclonal anti-histone H1 phosphorylated (Millipore, 06-597) were used. Goat antiRabbit IRDye 800WE (Li-COR) was used and detected using ODYSSEY Infrared Imaging System (Li-COR). Band intensities for histone were measured with ImageJ Software (NIH), and normalized to IgG heavy chain intensity. To evaluate the kinetic properties of the CDK5 phosphorylation, the reaction was performed with varying amounts of substrate (Histone concentrations ranging from 1 to 11.5 μM) and reaction was followed up to 35 min. V_o was calculated as the change in the normalized histone band intensity normalized to the intensity of the CDK5 band and then divided by the time observed in minutes to draw a Lineweaver-Burk projection.

Immunohistochemistry

Mouse brain sections (50 μm) were treated for 20 minutes on 0.1 M PB: Methanol (1:1), 1% hydrogen peroxide and incubated 1 h in 0.1 M PB with 1% BSA, 0.3% Triton X-100. Then the slices were incubated with mouse anti-Human-PHF-Tau (AT-8, 1:500, Pierce Biotechnology) mouse anti-Human-PHF-Tau (AT-8) primary antibody during overnight at $4\text{ }^{\circ}\text{C}$ in 0.1M PB with 0.3% BSA, 0.3% Triton X-100. Slices were incubated with biotinylated

mouse secondary antibody and then incubated with ABC-HRP complex (Pierce Biotechnology) for 2 h. Detection was developed with diaminobenzidine (DAB). The tissue was dehydrated and covered with mounting solution and observed by an Eclipse E200 optical microscope (Nikon).

Quantification of PHF-1 Immunoreactive Neurons in CA1

To analyze the effects of CDK5miR on the PHF-1-positive cells in the hippocampus of 3xTg-AD mice, we employed quantitative image analysis techniques using CLSM imaging of CA1. We used Hoechst labelling to automate the detection of cells in this area. First, we acquired 3D images on an Olympus FV-1000 CLS microscope using a 40× objective while imaging two channels: one for the Hoechst signal (350 nm) and the other for immunodetected PHF-1 stain (secondary antibody conjugated to Alexa 594). To analyze the whole CA1 area, we acquired two consecutive 3D images for each sample by manually panning the motorized stage; these 3D images were later automatically stitched together. The ultraviolet channel was used to automatically detect all nuclei present in the paired image and the red channel was used to classify all cells within the CA1 region expressing PHF-1.

The 3D stack alignment was performed automatically using an automatic registration and seamless mosaicking technique (Fedorov et al., 2002; Fedorov et al., 2006). We chose the translational transformation model considering deviations in rotation and scale introduced by the motorized stage being negligible. First, candidate locations were extracted as uniformly distributed local maxima over the condition surface (Kenney et al., 2003). Then for each of these locations the point descriptors were extracted. Considering small perturbations among input images, our choice sets the descriptors that can be computed efficiently. We use small circular windows whose intensity content was normalized and orientation was aligned with the average gradient orientation (Zuliani et al., 2004). Preliminary matches of the tie points were established identifying the pairs with minimum distance in the descriptor space. Afterwards, the inevitable outliers were pruned off using RANSAC-like algorithm producing final tie point matches. The transformation parameters were then estimated using matched tie points by the Normalized Direct Linear Transformation (DLT) algorithm (Hartley and Zisserman, 2004).

To blend stack planes together we used Multi-Resolution Splines (MRS) (Burt et al., 1983). Images were first decomposed into a multi-resolution Laplacian pyramid and the pyramids were then spliced level by level according to a weighted average over a transition zone. The blended image was obtained by reversely composing the spliced Laplacian pyramid. Therefore, the splice was matched to the scale of features and images were blended gradually without blurring finer image details. The averaged transition zone was identified by minimizing the error surface created by the absolute value of the difference of the gradients of overlapping areas (I_a and I_b). The approximate global solution for the minimization of the problem was given by a computationally efficient graph-cut algorithm (Boykov et al., 2001).

In all fused images, cell nuclei were automatically detected in the ultraviolet channel by a 3D Nuclei Detection algorithm (Obara et al., 2008). We focused on the pyramidal cells in CA1 and removed nuclei lying outside of this region by manually masking the region of interest, using open source Digital Notebook software (Kvilekval et al., 2010). The detection algorithm was divided into two steps: i) candidate location detection and ii) candidate location pruning. The nuclei centroid candidate locations were detected by local maxima of an image convolved with the 3D LoG kernel. The LoG kernel size is controlled by a user-defined average nuclear size parameter. The local maxima detection process continues by detecting locations of higher magnitude until the low intensity bound, defined by the user,

was reached. The candidate locations were then filtered in order to prune spurious locations due to circle-ellipsoid mismatch (we model nuclei as spheres), image noise and other issues. During this process all visible nuclei in the image were detected and indicated by a yellow outline.

The detected nuclei were classified according to PHF-1 expression in a small volume around each nucleus' centroid. Thus, each candidate location was described by computing the voxel intensity sum within the sphere constructed at that centroid location with a diameter 1.5 times larger than the nuclei diameter. Due to fluctuations in the intensity of PHF-1 penetration, expression and acquisition parameters we estimate the average background intensity of the PHF-1 signal by using Robust Median Absolute Deviation Estimator (Wang and Suter, 2004). This value is not affected by outliers to the same extent as the average estimation. Finally, the nuclei were classified using a modified K-means approach (Bishop, 1995), where one of the classes was bound by the robust median estimator. This approach avoids forcefully splitting nuclei into two classes if they lie below or above the PHF-1 background intensity. Cells classified as high PHF-1 after this analysis were indicated by a red outline. Small inserts in these figures zoom into an area of the CA1 nuclei, in order to emphasize the accuracy of the automated detection. An arrowhead was pointed to cells that belong to the high PHF-1 class, and we could visually confirm that the pointed cells express a high amount of PHF-1 immunoreactivity, noticed in the red pseudo-color of the image.

Statistical analyses

The *n* used for *in vitro* and *in vivo* experiments was 3–6. The parametric data were compared using multi-variable two-way analysis of variance (ANOVA) followed by Tukey's post-hoc test for comparison between several independent groups. A confidence level of $p < 0.05$ in a two-tailed test was adopted for statistical significance. The comparison between two groups was done using t-student test. Data were expressed as mean \pm S.E.M. Analyses were performed with SPSS (IBM company) and GraphPad Prism version 4.00. 2003 (GraphPad Software Inc., San Diego, CA).

Results

CDK5 RNAi Reduced Phosphorylated Tau *in vitro*

Following the model proposed by Chang K et al., 2006, we designed a microRNA that contains the backbone of the naturally occurring miR30, and the complementary sequence to target the CDK5 mRNA. This construct, referred to as shRNAmirCDK5 (or briefly, CDK5miR), was cloned in pCMV-GIN-ZEO.GFP plasmid (Open Biosystems). To validate the ability of our construct to knock down CDK5 expression *in vitro*, we transfected it into HEK 293T cells with lipofectamine 2000 reagent (Invitrogen) and detected transfected cells by GFP expression (figures 1a and 1c). Immunofluorescence of CDK5 was performed on transfected cultures, and we observed a decrease of the CDK5 immunofluorescence (IF) in transfected cells compared to untransfected cells present in the same optical field (figure 1d). Cells transfected with pCMV-GIN-ZEO.GFP plasmid carrying a scrambled version of the CDK5 targeting sequence, expressed the GFP protein, but did not show a change in the intensity of CDK5 fluorescence compared to untransfected cells present in the optical field (figure 1a, 1b). These observations were also evaluated by western blotting, and quantified by densitometry using Quantity One software version 4.6.0 (Biorad). We observed a significant decrease of CDK5 immunoreactivity of 76 ± 5.95 % in HEK 293T cells (figure 1e). Lentiviral particles were produced in HEK293T cells by co-transfecting the pCMV-GIN-ZEO plasmids containing either CDK5miR or SCRmiR, together with pMD2G and psPAX2 using calcium phosphate. Viral supernatants were recovered 2 days later, quantified by HIV p24 ELISA, Lentivirus Quantification Kit (Cell Biolabs, Inc), and titered by

transducing units (TU/mL) in HEK-293T (Naldini et al., 1996). Primary cultures of hippocampal neurons were transduced at DIV5 with these lentiviral particles (LV) at a titre of 10^9 LV/mL and at a MOI of 10. After 3 days the cultures were fixed with CB-PFA 4% and immunostained for CDK5 (figure 1f, 1h). In accord with observations made on HEK cells, LV-CDK5miR produced a reduction of CDK5 immunofluorescence in cells that expressed the reporter GFP, compared to untransduced (GFP-) cells (figure 1i). Cells transduced with LV carrying the scrambled construct showed no change in the CDK5 immunofluorescence (figure 1g). We estimated that the fluorescence intensity of CDK5 in CDK5miR transduced neurons differed significantly from those transduced with the control SCRmiR, showing a decrease of $52.5 \pm 3.38\%$ in CDK5miR treated cells (Figure 1j).

CDK5miR and SCRmiR in pCMV-GIN-ZEO.GFP plasmid were also transfected in neuronal cultures at DIV5 for 3 days (figure 2a, 2c) and stained for phosphorylated tau using AT-8 antibody (figure 2b, 2d). As shown in figure 2d and insert 2e, knocking down of CDK5 by transfection of CDK5miR reduced the AT-8 immunoreactivity in the neuritic processes, compared to that observed in transfected neurons with the SCRmiR (Insert 2e). Fluorescence intensity, quantified using the software image Scope-pro, showed significantly less immunofluorescence in neurons transfected with CDK5miR ($33,1 \pm 10,3\%$) compared to the neurons transfected with SCRmiR (figure 2f).

CDK5miR and SCRmiR synthetic microRNAs were cloned in the plasmid AAV-CMV.hrGFP, and adeno-associated viral particles serotype 2/5 were produced. Hippocampal neurons were transduced with these adeno-associated particles in DIV5 neurons at a titre of 10^{12} genomes per mL with a high efficiency of transduction. We obtained a monolayer of neurons that homogeneously expressed the viral transgenes, as seen by the GFP reporter (data not shown). After culturing the adeno-associated transduced neurons for 15 days with AAV-CDK5miR or AAV-SCRmiR, protein extracts were immuno-blotted for phosphorylated tau with PHF-1 antibody. In this experiment, we confirmed a significant reduction of the PHF-1 immunoreactive band in the neuronal primary cultures expressing the CDK5miR with respect to the SCRmiR as control (figure 2g, 2h).

We then sought to determine the effect of CDK5 knock-down on the subunits p35 and p25 in the same protein extracts of AAV transduced neurons. We confirmed a significant decrease of the CDK5 immunoreactivity; however, p35 and p25 were strikingly increased in the neuronal cultures expressing CDK5miR compared to SCRmiR cultures (figure 2g). CDK5 activity has been linked to the ratio between p25 and p35 (Patrick et al., 1999; Tseng, 2002). We determined that this ratio was not modified in the neuronal cultures treated with AAV-CDK5miR (figure 2h).

CDK5 RNAi Reduced Phosphorylated Tau *in vivo*

We next assayed *in vivo* the silencing of CDK5 on the levels of phosphorylated tau. We stereotactically injected lentiviral particles carrying CDK5miR or SCRmiR in the hippocampus of six month old C57BL/6 wild type mice. After sacrifice at 1 or 3 weeks post-injection, their hippocampi were dissected, homogenized, and protein extracts were analyzed by Western blotting to determine the levels of CDK5, phosphorylated tau with PHF-1 and pSer199 tau antibodies, and total tau with Tau-5 antibody. In the mice injected with LV-CDK5miR for one week, CDK5 was significantly reduced (figure 2i, 2j). However, at 3 weeks post-injection there was greater variability in the CDK5 immunoreactivity and the difference did not achieve significance. When tau immunoreactivity was analyzed at the same two points, the PHF-1 and p-ser199 tau signals were significantly decreased at three weeks, but not at one week. The expression of Tau-5 was not affected (Figure 2i, 2j). The delay in a decrease of tau phosphorylation relative to CDK5 knock-down may be due to the long half-life of the CDK5-induced phosphorylation sites. Taken together, these results

demonstrate that the CDK5miR mediated the knock down of CDK5 *in vivo* was associated with a reduction in the phosphorylation of tau.

We investigated the effect of CDK5miR *in vivo* in the triple transgenic Alzheimer's disease mouse model (3xTg-AD mice). At 18 months and older this murine model (Oddo et al, 2003) displays hippocampal neurofibrillary tangles similar to those in AD patients. We injected either AAV-CDK5miR or AAV-SCRmiR bilaterally into the hippocampi of 18 month old 3xTg-AD mice. These animals were sacrificed three weeks post-injection; one hemisphere was frozen and stored at -80°C , and the other was immersed in PFA 4% for 48 h, sectioned, and analyzed by fluorescence microscopy (IX 81, Olympus). In fixed cerebral tissues, we found that the 3xTg-AD mice treated with AAV-CDK5miR had a notable decrease of the CDK5 immunofluorescence in Dentate Gyrus, CA1, CA2 and CA3 areas with AAVCDK5miR transduction, compared with AAV-SCRmiR (figure 3).

The frozen tissue was slowly thawed on ice, the hippocampus dissected, homogenized, and protein extracts were analyzed by Western blotting. The AAVCDK5miR injected brains had a weak reduction in the CDK5 immunoreactive band. Despite this moderate effect on CDK5 levels *in vivo*, we confirmed that the phosphorylation of tau was strongly reduced by the CDK5miR treatment, i.e. the PHF-1 band detected in hippocampi of 3xTg-AD mice injected with CDK5miR resulted in a five-fold reduction compared to the band in mice treated with SCR-miR (figure 4a). In addition, p35 levels were significantly increased in mice treated with CDK5miR compared to the control SCRmiR. However, p25 did not show a comparable increase (figure 4a). To analyze the up-regulation of p35, CDK5 immunoprecipitation was performed from protein extracts of transduced neuronal cultures. We found that the increased p35 was in a pool that is not associated with CDK5 in the neurons treated with AAV-CDK5miR compared to the AAV-SCRmiR treated cells (Figure 4b).

CDK5 RNAi Decreased CDK5 Protein Availability without Affecting Kinase Activity

To determine whether CDK5 kinase activity was reduced by CDK5miR, we quantified kinase activity in the hippocampi of AAV-CDK5miR-treated 18–23 month old 3xTg-AD mice. CDK5 was immunoprecipitated and its steady state kinetics was studied using excess histone as substrate. In agreement with total lysates (figure 4a), lower amounts of CDK5 were detected in the immunoprecipitated fractions from CDK5miR injected mice compared to SCRmiR injected mice (figure 4c). The product formation of phosphorylated histone was observed over a 60 min time-course when incubated at 37°C in the presence of CDK5 from the CDK5miR- and SCRmiR-treated tissues, suggesting that the CDK5 remaining in the AAV-CDK5miR treated fraction was still functionally active (figure 4d). We then performed quantitative analysis using data obtained from western blots and results were presented in figure 4d. Data were fit to steady state linear expression, and the reaction rates were calculated according to the slope. We found a significant 50% product formation rate reduction after CDK5miR treatment of transgenic mice compared to control (Figure 4e). A significant 45% reduction was also found in replicate experiments done in wild type mice (figure 4f). This result might be due to reduced CDK5 availability alone or in combination with partially impaired kinase activity.

To answer this question, we performed the same *in vitro* assay as in the transgenic mice study, but varied concentrations of substrate at the 30 min time point when product formation was still linear, so the reaction rate was directly correlated with enzyme concentration in the assay. Enzyme concentration was normalized by the density of CDK5 observed in the immunoprecipitated fraction and results were plotted on a Lineweaver-Burk projection (Lineweaver and Burk, 1934). From three independent experiments average K_M and V_{MAX} were estimated as follows: with CDK5miR treatment $K_M = 4.02 \mu\text{M}$ and $V_{MAX} = 2.72 \pm 1.76 \text{ min}^{-1}$, with SCRmiR treatment $K_M = 2.71 \mu\text{M}$ and $V_{MAX} = 3.35 \pm 4.5 \text{ min}^{-1}$.

No apparent changes in the kinetic properties of the enzyme were observed (figure 4g). These findings suggest that a reduced amount of CDK5 following CDK5miR treatment led to reduced enzyme availability while CDK5 activity remained unchanged.

Silencing of CDK5 reduced the number of neurofibrillary tangles in the hippocampi of triple-transgenic Alzheimer mice

Triple transgenic Alzheimer's disease mice (3xTg-AD) had highly PHF-1 immunoreactive cells in the CA1 area of the hippocampus at 18–23 months old. Immunohistochemistry performed on 50 μ m coronal sections of the mouse brains showed PHF-1+ cells in mice 18 and 23 months old, using both fluorescence (PHF-1+ cells in green/nuclei in red by Hoechst) (figure 5a) and DAB (AT-8 positive cells) (figure 5b), as previously observed (Oddo et al 2003). In the 23 month old animals, PHF-1 immunoreactivity was stronger in the cellular cytoplasm surrounding the nucleus than in the younger 18 month old mice (insert frame in figure 5a). Eighteen month old mice had stronger PHF-1 immunoreactivity in neuritic processes compared to the 23 month old animals (figure 5c). When we injected AAV-CDK5miR intra-hippocampally and sacrificed the mice three weeks later, the extent of the tau pathology appeared to be reduced by immunodetection (figure 5d, 5e) compared to the SCRmiR injection (fig 5a, 5b). This finding was replicated in 18 month old mice (figure 5f). Therefore, silencing of CDK5 is capable of reducing the extent of tau pathology in mice at an advanced age.

To quantify the observed reduction in tau immunoreactivity we analyzed the sections with CLSM imaging of hippocampal CA1 in 3xTg-AD mice. Our goal was to quantify the number of cells with high PHF-1 expression in the CA1 area, in mice treated by intra-hippocampal injection of CDK5miR or SCRmiR. We acquired images from a total of 8 control mice injected with SCRmiR (Six, 18 month and two, 23 months old), and a total of 10 experimental mice injected with CDK5miR, six of the mice were 18 months and four of them 23 months old (figure 6a, 6b). All CA1 neurons in these images were automatically classified according to PHF-1 intensity in two classes: low and high PHF-1 immunoreactivity (figure 6c–6f), and the percentage of high PHF-1 cells to total cells were calculated. (Figure 6g). These automated quantitative analyses corroborated the findings observed in the figure 5. An average of 10.05 ± 1.3 % of cells in the CA1 region of 3xTg-AD mice were classified as high PHF-1 in control mice, whereas the CDK5miR intra-hippocampal treatment caused a significant reduction of cells classified as high PHF-1 in mice of the same age, reaching values as low as 2.7 ± 0.67 % (Fig 6g, left bars), which was supported by the single fluorescence quantification (Figure 6h). Interestingly, the density of cells in this area also differed. We detected more neurons in the CA1 area of 18–23 month old transgenic mice treated with CDK5miR, suggesting that the silencing of CDK5 might prevent the rapid loss of neurons in elder mice (figure 6g, right bars).

Discussion

The knock-down of CDK5 reduces the levels of phosphorylated tau, the number of neurofibrillary tangles and blocks the rapid neuronal loss in the hippocampi of elder triple transgenic mice. Based on our results, we propose CDK5 RNAi-mediated silencing as a novel gene therapy strategy against the tau pathology associated with Alzheimer's disease.

Several studies report CDK5 inhibition by pharmacological inhibitors such as, olomoucine, roscovitine, purvalanol, flavopiridol, butyrolactone, indirubins, hymenialdisine, the paullones and the aloisines (Garrett and Fattaey, 1999; Gray et al., 1999; Meijer et al., 1999; Leost et al., 2000; Sielecki et al., 2000; Knockaert et al., 2002; Mettey et al., 2003). Interestingly, hymenialdisine inhibits *in vivo* phosphorylation of tau at AD-specific sites in cultured insect cells (Meijer et al., 2000). Alsterpaullone, an inhibitor for CDK5 and

GSK-3 β inhibits the *in vivo* phosphorylation of tau at AD-specific sites in slices from mouse striatum (Leost et al., 2000). A notable disadvantage to all these inhibitors is that these are competitive inhibitors at the ATP binding site, resulting in a lack of specificity among the many ATP-dependent kinases. However, the shRNAmiCDK5 (CDK5miR) offers specific inhibition of CDK5. This study shows that CDK5 is a valid therapeutic target. The previous chemical inhibitors lacked the specificity as compared to RNAi. Therefore this is a proof-of-concept study, which suggests that RNAi is a valid therapeutic approach but also suggests that developing more specific inhibitors of CDK5 is a worthy goal.

We observed that 3 weeks CDK5miR treatment decreased the phosphorylated tau in adult brain of wild type mice. However, the CDK5 protein levels displayed tendency to recover at 3 weeks of treatment compared to one week. This may indicate an endogenous feedback operating to maintain the CDK5 necessary for its normal function in the nervous tissue. *In vivo* data of CDK5 kinetic showed normal activity after silencing of CDK5. We calculated a CDK5 K_M of 4 μ M with histone as substrate. This value is comparable to the previously described K_M of 4 μ M *in vivo* tau (Jae Suk Ahn et al., 2004) and K_M of 10 μ M *in vitro* for histone (Min Liu et al., 2008). A 45–50% reduction in the histone phosphorylation rate with CDK5 obtained from cerebral tissue of CDK5miR treated mice was associated with a comparable reduction of CDK5 in the same tissues. Based on these data, we suggest that diminution of the amount of CDK5 available in the tissue regulates or normalizes the activity of CDK5 in the transgenic mice, resulting in amelioration of the tau pathology.

We also observed increased p35 levels in the brain of 3xTg-AD mice treated with CDK5miR. Mice that over-express human p35, CDK5, and tau display increased CDK5 activity without an evident increase in tau phosphorylation (Van den Haute et al., 2001). These findings are consistent with our results and indicate that p35/CDK5 does not efficiently phosphorylate tau. However, recombinant p25/CDK5 phosphorylates tau with higher efficiency than p35/CDK5 *in vitro* (Hashiguchi et al., 2002). The 3xTg-AD mice treated with CDK5miR in our study had increased p35 and reduced CDK5. These circumstances may reduce p25-mediated CDK5 phosphorylation of tau. As a consequence a lower number of tangle bearing neurons were seen in treated mice, despite of their advanced age.

Recent studies show that p25/CDK5 deregulates histone deacetylase 1 (HCDAC1) activity inducing aberrant cell cycle and double-strand DNA breaks prior to neuronal death in CK-p25 mice (Kim et al., 2008). Other reports showed that conditional knockout of CDK5 in the adult mouse brain improved performance in spatial learning tasks, enhanced hippocampal long-term potentiation, and decreased CDK5-induced NR2B (NMDA subunit) degradation by calpain (Hawasli et al. 2007). Moreover, partial inhibition of CDK5 has been a proposed as therapeutic option (Camins et al., 2006; Zheng et al 2005).

Decreasing the availability of CDK5 could be a useful therapeutic approach. Excessive up-regulation of CDK5 by the truncated activators may contribute to neurodegeneration and alter the phosphorylation state of cytosolic and cytoskeletal proteins. Increased CDK5 activity has been implicated not only in Alzheimer's Disease (AD), but also in amyotrophic lateral sclerosis (ALS), Parkinson's disease, Niemann-Pick type C disease, ischemia and animal models with some of these conditions (Lee et al., 1999; Patrick et al., 1999; Nguyen et al., 2001; Bu et al., 2002; Lu et al., 2003; Nguyen and Julien, 2003; Smith et al., 2003; Wang et al., 2003). In summary, silencing CDK5 opens a novel gene therapy strategy to control the amount of CDK5 to reduce the tau pathology associated to Alzheimer's disease and other tauopathies.

Acknowledgments

We want to thank Dr. P. Davies at Feinstein Institute for Medical Research, Manhasset, NY for the donation of PHF-1 antibody. We extend our appreciation to Dr Xuemei Zhang at Neuroscience Research Institute, UCSB for her expert advice on the CDK5 enzyme assays. We thank Tania Marquez for assistance in maintaining the mouse and rats colonies in the SPF vivarium of the University of Antioquia. D. Piedrahita was recipient of a Doctoral Fellowship from Colciencias. This research was supported by: AG024024063 NIH-Fogarty R21 Project (KK and GPC-G), AG029802-01 RO1 NIA/NIH project (KK and GPC-G); Colciencias Projects # 11150418078 and #111545921503 (GPC-G); NIH NS 50210 project (BD and KK), Advanced Microscopy Unit and Viral Vector Core and Gene Therapy, Group of Neuroscience of Antioquia. University of Antioquia was also supported by: Colciencias Projects # 111540820511 and 111545921525 (JCG-G); CODI University of Antioquia, Colombia (GPC-G and JCG-G). Confocal imaging was done under the aegis of the Center for Bio-Image Informatics using an Olympus FV1000 CLSM microscope. The Center for Bio-Image Informatics is partially supported by the: NSF ITR (Information Technology Research) 0331697, NSF EIA-0080134, and NSF III-0808772.

References

- Arriagada PV, Growdon JH, Hedley-Whyte ET, Hyman BT. Neurofibrillary tangles but not senile plaques parallel duration and severity of Alzheimer's disease. *Neurology*. 1992; 42:631–639. [PubMed: 1549228]
- Augustinack JC, Schneider A, Mandelkow EM, Hyman BT. Specific tau phosphorylation sites correlate with severity of neuronal cytopathology in Alzheimer's disease. *Acta Neuropathol*. 2002; 103:26–35. [PubMed: 11837744]
- Banker, G.; Kimberly, G. *Culturing Nerve Cells*. 2nd edition. The MIT press; London: 2002.
- Banker, G.; Kimberly, G. *Culturing Nerve Cells*. 2nd edition. The MIT press; London: 2002.
- Baumann K, Mandelkow EM, Biernat J, Piwnica-Worms H, Mandelkow E. Abnormal Alzheimer-like phosphorylation of tau-protein by cyclin-dependent kinases cdk2 and cdk5. *FEBS Lett*. 1993; 336:417–424. [PubMed: 8282104]
- Bishop, CM. *Neural Networks for Pattern Recognition*. Oxford University Press; 1995.
- Braak E, Braak H, Mandelkow EM. A sequence of cytoskeleton changes related to the formation of neurofibrillary tangles and neuropil threads. *Acta Neuropathol*. 1994; 87:554–567. [PubMed: 7522386]
- Boudreau, RL; Monteys, AM.; Davidson, BL. Minimizing variables among hairpin-based RNAi vectors reveals the potency of shRNAs. *RNA*. 2008; 14(9):1834–44. [PubMed: 18697922]
- Boudreau RL, McBride JL, Martins I, Shen S, Xing Y, Carter BJ, Davidson BL. Nonallele-specific silencing of mutant and wild-type huntingtin demonstrates therapeutic efficacy in Huntington's disease mice. *Mol Ther*. 2009; 17:1053–63. [PubMed: 19240687]
- Boykov Y, Kolmogorov V. An Experimental Comparison of Min-cut/Max-ow Algorithms for Energy Minimization in Vision. *Energy Minimiz. Meth. in Comp. Vis. and Patt. Recog*. 2001; 359:374.
- Bu B, Li J, Davies P, Vincent I. Deregulation of cdk5, hyperphosphorylation, and cytoskeletal pathology in the Niemann-Pick type C murine model. *J Neurosci*. 2002; 22:6515–6525. [PubMed: 12151531]
- Burt PJ, Adelson EH. A Multiresolution Spline with Application to Image Mosaics. *ACM Transactions on Graphics*. 1983; 2:217–236.
- Camins A, Verdaguer E, Folch J, Canudas AM, Pallàs M. The role of CDK5/P25 formation/inhibition in neurodegeneration. *Drug News Perspect*. 2006; 19(8):453–60. [PubMed: 17160145]
- Cardona-Gomez P, Perez M, Avila J, Garcia-Segura LM, Wandosell F. Estradiol inhibits GSK3 and regulates interaction of estrogen receptors, GSK3, and beta-catenin in the hippocampus. *Mol Cell Neurosci*. 2004; 25:363–373. [PubMed: 15033165]
- Chang K, Elledge SJ, Hannon GJ. Lessons from Nature: microRNA-based shRNA libraries. *Nat Methods*. 2006; 3:707–714. [PubMed: 16929316]
- Churcher I. Tau therapeutic strategies for the treatment of Alzheimer's disease. *Curr Top Med Chem*. 2006; 6:579–595. [PubMed: 16712493]
- Cruz JC, Tseng HC, Goldman JA, Shih H, Tsai LH. Aberrant Cdk5 activation by p25 triggers pathological events leading to neurodegeneration and neurofibrillary tangles. *Neuron*. 2003; 40:471–483. [PubMed: 14642273]

- Dhavan R, Tsai LH. A decade of CDK5. *Nat Rev Mol Cell Biol.* 2001; 2:749–759. [PubMed: 11584302]
- Fedorov, D.; Fonseca, LM.; Kenney, C.; Manjunath, BS. Automatic registration and mosaicking system for remotely sensed imagery. *SPIE 9th International Symposium on Remote Sensing*; 2002.
- Fedorov, D.; Sumengen, B.; Manjunath, BS. Multi-focus imaging using local focus estimation and mosaicking. *IEEE International Conference on Image Processing (ICIP06)*; 2006.
- Fischer PM. Recent advances and new directions in the discovery and development of cyclin-dependent kinase inhibitors. *Curr Opin Drug Discov Devel.* 2001; 4:623–634.
- Gallego-Gomez JC, Risco C, Rodriguez D, Cabezas P, Guerra S, Carrascosa JL, Esteban M. Differences in virus-induced cell morphology and in virus maturation between MVA and other strains (WR, Ankara, and NYCBH) of vaccinia virus in infected human cells. *J Virol.* 2003; 77:10606–10622. [PubMed: 12970445]
- Garrett MD, Fattaey A. CDK inhibition and cancer therapy. *Curr Opin Genet Dev.* 1999; 9:104–111. [PubMed: 10072351]
- Gong CX, Iqbal K. Hyperphosphorylation of microtubule-associated protein tau: a promising therapeutic target for Alzheimer disease. *Curr Med Chem.* 2008; 15:2321–2328. [PubMed: 18855662]
- Gray N, Detivaud L, Doerig C, Meijer L. ATP-site directed inhibitors of cyclin-dependent kinases. *Curr Med Chem.* 1999; 6:859–875. [PubMed: 10495356]
- Hartley, RI.; Zisserman, A. *Multiple View Geometry in Computer Vision*. second edition. Cambridge University Press; 2004.
- Hashiguchi M, Saito T, Hisanaga S, Hashiguchi T. Truncation of CDK5 activator p35 induces intensive phosphorylation of Ser202/Thr205 of human tau. *J Biol Chem.* 2002; 277:44525–44530. [PubMed: 12226093]
- Hawasli AH, Benavides DR, Nguyen C, Kansy JW, Hayashi K, Cambon P, Greengard P, Powell CM, Cooper DC, Bibb JA. Cyclin-dependent kinase 5 governs learning and synaptic plasticity via control of NMDAR degradation. *Nat neurosci.* 2007; 10:880–886. [PubMed: 17529984]
- Iqbal K, Alonso Adel C, Chen S, Chohan MO, El-Akkad E, Gong CX, Khatoon S, Li B, Liu F, Rahman A, Tanimukai H, Grundke-Iqbal I. Tau pathology in Alzheimer disease and other tauopathies. *Biochim Biophys Acta.* 2005; 1739:198–210. [PubMed: 15615638]
- Ahn, Jae Suk; Musacchio, Andrea; Mapelli, Marina; Ni, Jake; Scinto, Leonard; Stein, Ross; Kosik, Kenneth S.; Yeh, Li-An. Development of an Assay to Screen for Inhibitors of Tau Phosphorylation by Cdk5. *J Biomol Screen.* 2004; 9:122–131. [PubMed: 15006135]
- Kenney CS, Manjunath BS, Zuliani M, Hewer MGA, Nevel AV. A condition number for point matching with application to registration and postregistration error estimation. *IEEE T. on Pattern Analysis and Mach. Intel.* 2003; 25(11):1437–1454.
- Kim D, Frank CL, Dobbin M, Tsunemoto RK, Tu Weighong, Peng Peter L, Guan Ji-song, Lee BH, Moy LY, Giusti P, Broodie N, Mazitschek R, Delalle I, Haggarty S, Neve RL, Lu Y, Tsai LH. Dereglatin of HDAC1 by p25/Cdk5 in Neurotoxicity. *Neuron.* 2008; 60(5):803–817. [PubMed: 19081376]
- Knockaert M, Greengard P, Meijer L. Pharmacological inhibitors of cyclin-dependent kinases. *Trends Pharmacol Sci.* 2002; 23:417–425. [PubMed: 12237154]
- Kobayashi S, Ishiguro K, Omori A, Takamatsu M, Arioka M, Imahori K, Uchida T. A cdc2-related kinase PSSALRE/cdk5 is homologous with the 30 kDa subunit of tau protein kinase II, a proline-directed protein kinase associated with microtubule. *FEBS Lett.* 1993; 335:171–175. [PubMed: 8253190]
- Kusakawa F, Saito T, Onuki R, Ishiguro K, Kishimoto T, Hisanaga S. Calpain-dependent proteolytic cleavage of the p35 cyclin-dependent kinase 5 activator to p25. *J Biol Chem.* 2000; 275:17166–17172. [PubMed: 10748088]
- Kvilekval K, Fedorov D, Obara B, Singh A, Manjunath BS. Bisque: A Platform for Bioimage Analysis and Management. *Bioinformatics.* 2010; 26:544–552. [PubMed: 20031971]

- Lee KY, Clark AW, Rosales JL, Chapman K, Fung T, Johnston RN. Elevated neuronal Cdc2-like kinase activity in the Alzheimer disease brain. *Neurosci Res.* 1999; 34:21–29. [PubMed: 10413323]
- Leost M, Schultz C, Link A, Wu YZ, Biernat J, Mandelkow EM, Bibb JA, Snyder GL, Greengard P, Zaharevitz DW, Gussio R, Senderowicz AM, Sausville EA, Kunick C, Meijer L. Paullones are potent inhibitors of glycogen synthase kinase-3beta and cyclin-dependent kinase 5/p25. *Eur J Biochem.* 2000; 267:5983–5994. [PubMed: 10998059]
- Lew J, Huang QQ, Qi Z, Winkfein RJ, Aebersold R, Hunt T, Wang JH. A brain-specific activator of cyclin-dependent kinase 5. *Nature.* 1994; 371:423–426. [PubMed: 8090222]
- Lineweaver H, Burk D. The Determination of Enzyme Dissociation Constants. *Journal of the American Chemical Society.* 1934; 56:658–666.
- Lu L, Grimm JW, Shaham Y, Hope BT. Molecular neuroadaptations in the accumbens and ventral tegmental area during the first 90 days of forced abstinence from cocaine self-administration in rats. *J Neurochem.* 2003; 85:1604–1613. [PubMed: 12787079]
- Mazanetz MP, Fischer PM. Untangling tau hyperphosphorylation in drug design for neurodegenerative diseases. *Nat Rev Drug Discov.* 2007; 6:464–479. [PubMed: 17541419]
- Meijer L, Thunnissen AM, White AW, Garnier M, Nikolic M, Tsai LH, Walter J, Cleverley KE, Salinas PC, Wu YZ, Biernat J, Mandelkow EM, Kim SH, Pettit GR. Inhibition of cyclin-dependent kinases, GSK-3beta and CK1 by hymenialdisine, a marine sponge constituent. *Chem Biol.* 2000; 7:51–63. [PubMed: 10662688]
- Mettey Y, Gompel M, Thomas V, Garnier M, Leost M, Ceballos-Picot I, Noble M, Endicott J, Vierfond JM, Meijer L. Aloisines, a new family of CDK/GSK-3 inhibitors. SAR study, crystal structure in complex with CDK2, enzyme selectivity, and cellular effects. *J Med Chem.* 2003; 46:222–236. [PubMed: 12519061]
- Liu, Min; Choi, Sungwoon; Cuny, Gregory D.; Ding, Kai; Dobson, Brittany C.; Glicksman, Marcie A.; Auerbach, Ken; Stein, Ross L. Kinetic Studies of Cdk5/p25 Kinase: Phosphorylation of Tau and Complex Inhibition by Two Prototype Inhibitors. *Biochemistry.* 2008; 47:8367–8377. [PubMed: 18636751]
- Morishima-Kawashima M, Hasegawa M, Takio K, Suzuki M, Yoshida H, Titani K, Ihara Y. Proline-directed and non-proline-directed phosphorylation of PHF-tau. *J Biol Chem.* 1995; 270:823–829. [PubMed: 7822317]
- Naldini L, Blomer U, Gallay P, Ory D, Mulligan R, Gage FH, Verma IM, Trono D. In vivo gene delivery and stable transduction of nondividing cells by a lentiviral vector. *Science.* 1996; 272:263–267. [PubMed: 8602510]
- Nguyen MD, Julien JP. Cyclin-dependent kinase 5 in amyotrophic lateral sclerosis. *Neurosignals.* 2003; 12:215–220. [PubMed: 14673208]
- Nguyen MD, Lariviere RC, Julien JP. Dereglulation of Cdk5 in a mouse model of ALS: toxicity alleviated by perikaryal neurofilament inclusions. *Neuron.* 2001; 30:135–147. [PubMed: 11343650]
- Noble W, Olm V, Takata K, Casey E, Mary O, Meyerson J, Gaynor K, LaFrancois J, Wang L, Kondo T, Davies P, Burns M, Veeranna Nixon R, Dickson D, Matsuoka Y, Ahljanian M, Lau LF, Duff K. Cdk5 is a key factor in tau aggregation and tangle formation in vivo. *Neuron.* 2003; 38:555–565. [PubMed: 12765608]
- Obara, B.; Byun, J.; Fedorov, D.; Manjunath, BS. Automatic nuclei detection and data flow in bisquik system. Workshop on Bio-Image Informatics: Biological Imaging, Computer Vision and Data Mining. 2008. <http://dough.ece.ucsb.edu/nuclei3d/>
- Oddo S, Caccamo A, Shepherd JD, Murphy MP, Golde TE, Kaye R, Metherate R, Mattson MP, Akbari Y, LaFerla FM. Triple-transgenic model of Alzheimer's disease with plaques and tangles: intracellular Abeta and synaptic dysfunction. *Neuron.* 2003; 39:409–421. [PubMed: 12895417]
- Patrick GN, Zukerberg L, Nikolic M, de la Monte S, Dikkes P, Tsai LH. Conversion of p35 to p25 deregulates Cdk5 activity and promotes neurodegeneration. *Nature.* 1999; 402:615–622. [PubMed: 10604467]

- Paudel HK, Lew J, Ali Z, Wang JH. Brain proline-directed protein kinase phosphorylates tau on sites that are abnormally phosphorylated in tau associated with Alzheimer's paired helical filaments. *J Biol Chem.* 1993; 268:23512–23518. [PubMed: 8226879]
- Shiradkar MR, Padhalingappa MB, Bhetalabhotla S, Akula KC, Tupe DA, Pinninti RR, Thummanagoti S. A novel approach to cyclin-dependent kinase 5/p25 inhibitors: A potential treatment for Alzheimer's disease. *Bioorg Med Chem.* 2007; 15:6397–6406. [PubMed: 17643991]
- Sielecki TM, Boylan JF, Benfield PA, Trainor GL. Cyclin-dependent kinase inhibitors: useful targets in cell cycle regulation. *J Med Chem.* 2000; 43:1–18. [PubMed: 10633033]
- Silva JM, Li MZ, Chang K, Ge W, Golding MC, Rickles RJ, Siolas D, Hu G, Paddison PJ, Schlabach MR, Sheth N, Bradshaw J, Burchard J, Kulkarni A, Cavet G, Sachidanandam R, McCombie WR, Cleary MA, Elledge SJ, Hannon GJ. Second-generation shRNA libraries covering the mouse and human genomes. *Nat Genet.* 2005; 37:1281–1288. [PubMed: 16200065]
- Skovronsky DM, Lee VM, et al. Neurodegenerative diseases: new concepts of pathogenesis and their therapeutic implications. *Annu Rev Pathol.* 2006; 1:151–70. [PubMed: 18039111]
- Smith PD, Crocker SJ, Jackson-Lewis V, Jordan-Sciutto KL, Hayley S, Mount MP, O'Hare MJ, Callaghan S, Slack RS, Przedborski S, Anisman H, Park DS. Cyclin-dependent kinase 5 is a mediator of dopaminergic neuron loss in a mouse model of Parkinson's disease. *Proc Natl Acad Sci U S A.* 2003; 100:13650–13655. [PubMed: 14595022]
- Stegmeier F, Hu G, Rickles RJ, Hannon GJ, Elledge SJ. A lentiviral microRNA-based system for single-copy polymerase II-regulated RNA interference in mammalian cells. *Proc Natl Acad Sci U S A.* 2005; 102:13212–13217. [PubMed: 16141338]
- Tang D, Yeung J, Lee KY, Matsushita M, Matsui H, Tomizawa K, Hatase O, Wang JH. An isoform of the neuronal cyclin-dependent kinase 5 (Cdk5) activator. *J Biol Chem.* 1995; 270:26897–26903. [PubMed: 7592934]
- Tsai LH, Delalle I, Caviness VS Jr, Chae T, Harlow E. p35 is a neural-specific regulatory subunit of cyclin-dependent kinase 5. *Nature.* 1994; 371:419–423. [PubMed: 8090221]
- Tseng HC, Zhou Y, Shen Y, Tsai LH. A survey of Cdk5 activator p35 and p25 levels in Alzheimer's disease brains. *FEBS Letters.* 2002; 523(1–3):58–62. [PubMed: 12123804]
- Urabe M, Ding C, Kotin RM. Insect cells as a factory to produce adeno-associated virus type 2 vectors. *Hum Gene Ther.* 2002; 13:1935–1943. [PubMed: 12427305]
- Van den Haute C, Spittaels K, Van Dorpe J, Lasrado R, Vandezande K, Laenen I, Geerts H, Van Leuven F. Coexpression of human cdk5 and its activator p35 with human protein tau in neurons in brain of triple transgenic mice. *Neurobiol Dis.* 2001; 8:32–44. [PubMed: 11162238]
- Wang H, Suter D. Robust Adaptive-Scale Parametric Model Estimation for Computer Vision. *IEEE Transactions on Pattern Analysis and Machine Intelligence.* 2004; 26(11):1459–1474. [PubMed: 15521494]
- Wang J, Liu S, Fu Y, Wang JH, Lu Y. Cdk5 activation induces hippocampal CA1 cell death by directly phosphorylating NMDA receptors. *Nat Neurosci.* 2003; 6:1039–1047. [PubMed: 14502288]
- Yu Y, Run X, Liang Z, Li Y, Liu F, Liu Y, Iqbal K, Grundke-Iqbal I, Gong CX. Developmental regulation of tau phosphorylation, tau kinases, and tau phosphatases. *J Neurochem.* 2009; 108:1480–94. [PubMed: 19183272]
- Zheng YL, Kesavapany S, Gravell M, Hamilton RS, Schubert M, Amin N, Albers W, Grant P, Pant HC. A Cdk5 inhibitory peptide reduces tau hyperphosphorylation and apoptosis in neurons. *EMBO J.* 2005; 24:209–20. [PubMed: 15592431]
- Zufferey, R.; Trono, D. *Current Protocols in Neurosciences*, unit 4.21, or *Current Protocols in Human Genetics*, unit 12.10. John Wiley & Sons ed.; New York: 2000. Production of high titer Lentiviral vectors.
- Zuliani M, Kenney C, Manjunath BS. A Mathematical Comparison of Point Detectors. *Second IEEE Image and Video Registration Workshop.* 2004

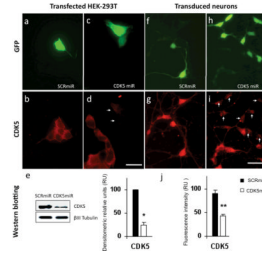


Figure 1. Knockdown of CDK5 in HEK-293T cell line and neuronal primary cultures by CDK5miR constructs

a) GFP expression of HEK-293T cells transfected with pCMV-GIN-ZEO-shRNAmirSCR.GFP (SCRmiR). b) CDK5 immunofluorescence in HEK-293T cells transfected with SCRmiR. c) GFP expression of HEK-293T cells transfected pCMV-GIN-ZEO-shRNAmirCDK5.GFP (CDK5miR). d) CDK5 immunofluorescence in HEK-293T cells transfected with CDK5miR; arrows point to GFP+ cells in panel c. Decrease of the CDK5 immunoreactivity is observed in transfected cells. Green: GFP fluorescence, red: Alexa 594. 60 \times , scale bar: 20 μ m. n=6. e) CDK5 Western blotting in HEK-293T transfected cells with SCRmiR and CDK5miR. A representative plot is shown. β III-Tubulin was used as loading control. Data is presented as mean \pm S.E.M. n=6, * = p<0,05. f) GFP expression of neuronal primary cultures transduced with LV- SCRmiR. g) Immunofluorescence of CDK5 in transduced neurons with LV-SCRmiR. h) GFP expression of neuronal primary cultures transduced with LV-CDK5miR. i) CDK5 immunofluorescence in neurons transduced with LV-CDK5miR. Arrows point to GFP+ transduced neurons seen in panel h. Decrease of CDK5 immunoreactivity in transduced neurons with LV-CDK5miR is observed. Green: GFP fluorescence, red: Alexa 594. 60 \times , scale bar: 20 μ m. n=6, ** = p<0,001. j) Quantification of the fluorescence intensity of CDK5 immunoreactivity of neurons transduced with LV-SCRmiR and LV-CDK5miR, using the software image scope pro, Media cybernetics. RU= Relative Units, n=6, ** = p<0,001.

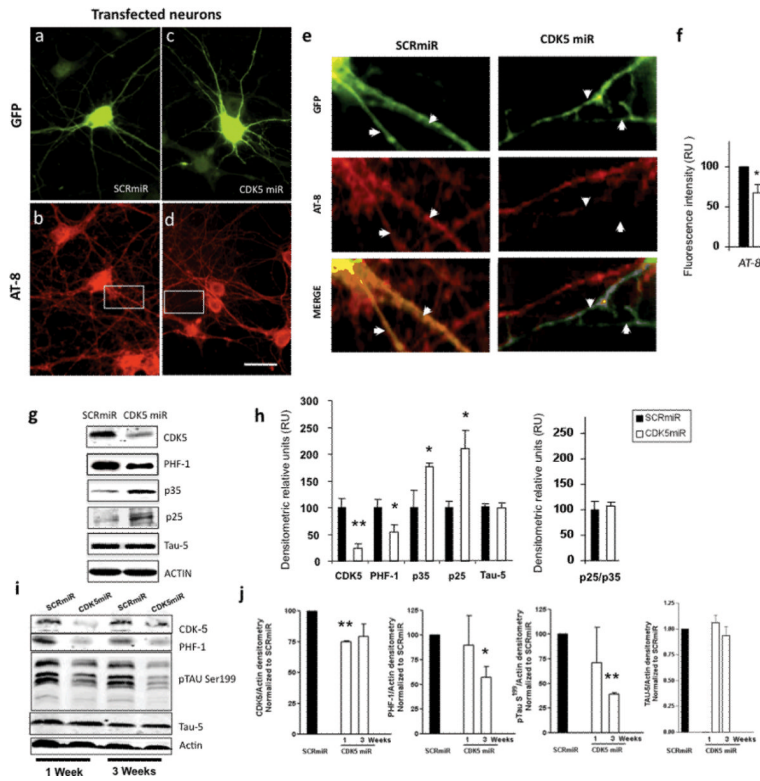


Figure 2. CDK5miR decreased the levels of phosphorylated tau

a) GFP expression of hippocampal neurons transfected with pCMV-GIN-ZEO.shRNA_{mir}SCR.GFP (SCRmiR). b) Immunofluorescence of phosphorylated tau with AT-8 antibody in neurons transfected with SCRmiR expressed in pCMV-GIN-ZEO-GFP plasmid. c) GFP expression of hippocampal neurons transfected with pCMV-GIN-ZEO.shRNA_{mir}CDK5.GFP (CDK5miR). d) Immunofluorescence of phosphorylated tau with AT-8 antibody in neurons transfected with CDK5miR; A decrease in AT-8 immunoreactivity was detected. Green: GFP fluorescence, red: Alexa 594. 60×, scale bar: 20 μm. n=4. e) Zoom inserts from b and d. Arrows indicate neuritic processes of transfected cells. The phospho-tau (AT-8) immunoreactivity decrease in neurites transfected with CDK5miR (GFP positive cells). f) Quantification of the fluorescence intensity of AT-8 immunoreactivity in neurons transfected with CDK5miR and SCRmiR, using the software image Scope-Pro (Media cybernetics). RU= Relative Units, n=4, * = p<0,05. g) CDK5, PHF-1, p35, and p25 were evaluated by Western Blotting in neuronal primary cultures transduced with AAV-CDK5miR and AAV-SCRmiR. β-actin was used as loading control. Representative blots are shown. h) Densitometric quantification from g, p25/p35 Ratio was calculated. Data are presented as mean ±S.E.M. p25 and p35 densitometry values were previously normalized to β-actin. n=6, * = p< 0,05. i) CDK5, PHF-1 tau, pSer199 tau and Tau-5 Western blotting from hippocampal lysates of C57BL6 mice injected with LV-CDK5miR and LV-SCRmiR. Representative blots are shown. j) Densitometry of Western blots in LV-CDK5miR and LV-SCRmiR treated mice was measured and normalized to actin. Data is plotted as the percentage of change between control (SCRmiR) and treated (CDK5miR) groups and presented as mean ±S.E.M. n=4, * = p< 0,05, **=p<0,001

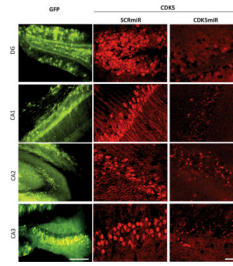


Figure 3. CDK5miR reduces CDK5 expression in the brain of triple transgenic Alzheimer mice 3xTg-AD mice (18–23 months old) were sacrificed three weeks after injection with AAV. Silencing of CDK5 expression by CDK5miR in the Dentate gyrus, CA1, CA2 and CA3 regions of 3xTg-AD mice. GFP represent the transduced areas in the hippocampus. 15 \times , scale bar: 100 μ m. CDK5 immunofluorescence 40 \times , scale bar 50 μ m. n=6.

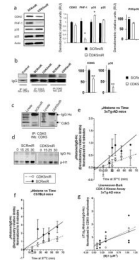


Figure 4. CDK5miR reduces CDK5 levels in the hippocampus of triple transgenic Alzheimer mice without affecting its kinetic activity

a) CDK5, PHF-1, p35, and p25 Western blotting from hippocampus of 3xTg-AD mice treated with SCRmiR and CDK5miR. β -actin as loading control. Representative blots are shown. Densitometric quantification was done, RU= Relative units. $n=3$, $*= p<0.05$. b) CDK5 Immunoprecipitation (IP), Wb: CDK5, p35 of neuronal primary cultures. A band corresponding to the IgG heavy chain was detected and used as loading control. Negative for IgG immunoprecipitation was used as an internal control. Representative blots are shown. Densitometric quantification of CDK5 and p35 proteins was done, RU= Relative units. $n=3$, $*= p<0.05$. c) CDK5 IP, Wb: CDK5 from hippocampus of 3xTg-AD mice treated with SCRmiR and CDK5miR. d) Temporal course for CDK5 kinase activity was detected by phosphorylated histone antibody. A band corresponding to the IgG heavy chain was detected. e) Product formation using CDK5 IP from hippocampi of transgenic and e) wild type mice was measured by densitometry and plotted against the reaction time. Linear regression was used and the fitting line was drawn (GraphPad Software). SCRmiR is shown as closed circles and a straight line, and CDK5miR is shown as open circles and a dotted line. Data is presented as mean \pm S.E.M. $n=3$. $*=p<0,05$. g) Phospho-histone formation was calculated as indicated above in several assays where substrate concentration was varied and normalized to CDK5 densitometry in the immunoprecipitation. Reaction rates were measured as the slope of the curve and Lineweaver-burk plot is graphed. Each value is presented in the dot-plot and lineal regression was used to fit the model. CDK5miR is shown as closed circles and a straight line, and SCRmiR is shown as open circles and a dotted line.

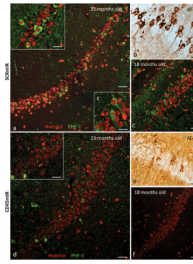


Figure 5. CDK5miR decreases phosphorylated tau and neurofibrillary tangles in 3xTg-AD mice
 a) Phospho-tau (PHF-1) immunofluorescence showing neurofibrillary tangles (NFTs) positive cells and b) phospho-tau (AT-8) immunoreactive cells present in the CA1 area of hippocampus of 23 month old 3xTg-AD mice three weeks post-injection with AAV-SCRmiR. c) PHF-1 immunofluorescence showing positive cells in CA1 in hippocampus of 18 month old 3xTg-AD mice, three weeks after hippocampal injection with AAV-SCRmiR. d) PHF-1 immunofluorescence and e) AT-8 immunoreactive cells in the CA1 area of 23 months old and f) 18 months old 3xTg-AD mice three weeks after injection with CDK5miR. n=6, Red pseudo-color: nucleus staining with Hoechst, green pseudo-color: PHF-1 IF, Alexa 594. 60 \times , Bar: 50 μ m; Inserts a, c, d: 100 \times , scale bar: 20 μ m.

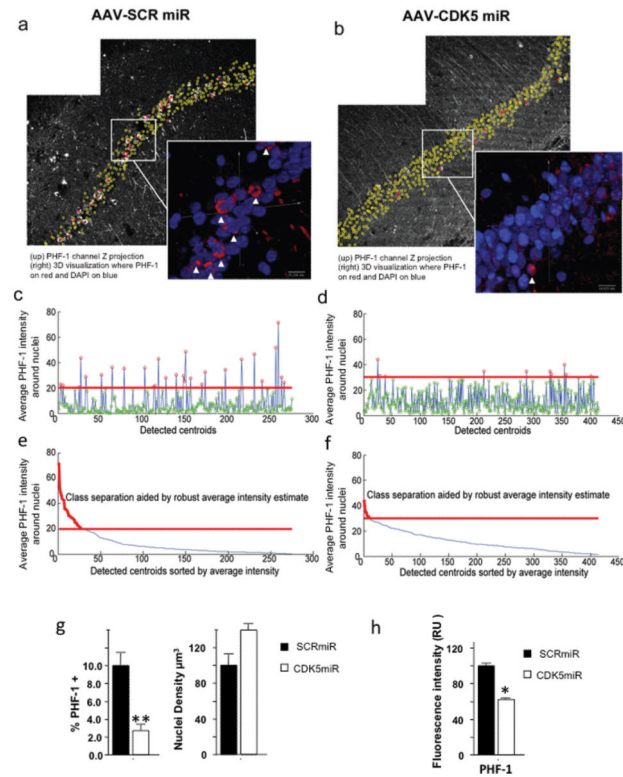


Figure 6. Silencing of CDK5 reduced the number of neurofibrillary tangles in the hippocampus of triple-transgenic Alzheimer mice

In this figure, left side images a), c) and e) correspond to AAV-SCRmiR and the right side b), d) and f) correspond to AAV-CDK5miR injection. Representative PHF-1 channels of hippocampal CA1 region of 23 months old 3xTg-AD mice, imaged three weeks after a) AAV-SCRmiR or b) AAV-CDK5miR injection. Inserted panels show magnified 3D visualizations of CA1 cell nuclei, generated using bioView3D software (Kvilekval et al., 2010), where, PHF-1 channel is shown in red and Hoechst is in blue. Arrows point towards cells automatically classified as high PHF-1. Plots c) and d) show average PHF-1 intensities within detected cells where point color represents the classification result, red indicates high PHF-1 and green indicates low PHF-1. The red line separates the classes. Plots e) and f) show the same data sorted according to the average intensity, where the plot portion colored in red is classified as high PHF-1. Note, that the CDK5miR image set was acquired at 1.5 times higher PMT voltage and offset than the SCRmiR. The bar graph g) shows a significant difference in the percentage of CA1 cells classified as high PHF-1 for both conditions (left). The density of the detected nuclei (right) shows a tendency to increase in old mice treated with CDK5miR; h) Intensity fluorescence quantification of PHF-1 also decreased after CDK5miR treatment. Data is presented as mean \pm S.E.M. n=8 to controls and n=10 to treated. * $p < 0,05$, ** $p < 0,001$.